Theor. Comput. Fluid Dyn.
DOI 10.1007/s00162-011-0243-9

ORIGINAL ARTICLE

T. A. Lavin · S. S. Girimaji · S. Suman · H. Yu

Flow-thermodynamics interactions in rapidly-sheared compressible turbulence

Received: 3 March 2011 / Accepted: 29 October 2011

Abstract We investigate the behavior of flow variables, thermodynamic variables and their interaction in rapidly sheared (S) homogeneous compressible turbulence using rapid distortion theory (RDT). We subject an initially isotropic and incompressible flow field to homogeneous shear-rate of various strengths quantified by a gradient Mach number (M_g) based on characteristic wavenumber. Our objective is to characterize the behavior of flow/thermodynamic fluctuations and their linear interactions during the course of turbulence evolution. Even though the mean shear-rate is held constant, the gradient Mach number progressively diminishes with time as the relevant wavenumber increases due to the mean deformation. The evolution exhibits three distinct phases which we categorize based on the character of pressure as: (i) Pressure-released (PR) stage which is observed when $St < \sqrt{M_{g0}}$ and pressure effects are negligible; (ii) Wave-character (WC) stage wherein $\sqrt{M_{g0}} < St < M_{g0}$ and the wave character of pressure is in evidence; and (iii) Low-Mach number (LM) stage when $St > M_{g0}$, where M_{g0} is the initial gradient Mach number. In the PR regime we find that the thermodynamic fluctuations evolve from their initial state but velocity fluctuations grow unhindered by pressure fluctuations. In the WC regime, the pressure fluctuations become significant and flow-thermodynamic interaction commences. This interaction brings about equipartition of dilatational kinetic energy and thermodynamic potential energy. The interaction also results in stabilization of turbulence, and the total kinetic energy growth comes to a near standstill. Ultimately in the LM stage, kinetic energy starts increasing again with the growth rate being very similar to that in incompressible RDT. However, the thermodynamic fluctuations continue to grow despite the gradient Mach number being substantially smaller than unity. Overall, the study yields valuable insight into the linear processes in high Mach number shear flows and identifies important closure modeling issues.

Keywords Compressible turbulence · Rapid-distortion theory · Turbulence modeling

Communicated by S. Sarkar.

T. A. Lavin
Sandia National Laboratory, Albuquerque, NM 87213, USA

S. S. Girimaji (✉) · S. Suman
Aerospace Engineering Department, Texas A&M University, College Station, TX 77843-3141, USA
E-mail: girimaji@aero.tamu.edu

S. Suman
E-mail: sawan.suman@gmail.com

H. Yu
Mechanical Engineering Department, John Hopkins University, Baltimore, MD 21218-2682, USA

Published online: 18 November 2011

1 Introduction

The inherent complexity of turbulence is further compounded in compressible flows by the dynamic coupling between flow and thermodynamic variables. In incompressible flows, pressure is merely a Lagrange multiplier with the sole function of maintaining a divergence-free velocity field. Evolution of incompressible turbulence is governed entirely by the momentum conservation equation subject to the kinematic incompressibility constraint. However, in compressible flows, pressure evolves according to a wave equation leading to profound changes in turbulence physics including tight coupling between velocity fluctuations and those of pressure, temperature, and density. As in the case of any compressible flow, compressible turbulence can be classified into different types based on the applicable state equation. Possible categories of compressible turbulence classification, in order of increasing complexity, are: (i) isothermal; (ii) isentropic; (iii) ideal gas and (iv) real gas. Barotropic flows (isothermal and isentropic) are the simplest of compressible flows. In barotropic turbulent flows, pressure is a direct function of density, and the energy equation is redundant. At the other extreme, flows under the influence of real gas effects represent the most complex form of compressible turbulence. Unfortunately, these flows do not easily lend themselves to fundamental analytical investigation. In this work, we will consider ideal gas compressible turbulence, which is of intermediate degree of complexity and yet of great utility. The extent of flow-thermodynamics coupling, given a state equation, depends upon factors such as Mach number, type of mean-velocity gradient, intensity of thermodynamic fluctuations, etc. It has been known for some time now that compressibility, in general, has a stabilizing influence on shear flow turbulence (e.g., [5,15,22]). To a large extent, the compressibility effects manifest via the pressure-strain correlation [25] and there have been efforts [1,11] to model this tensor and its trace—pressure-dilatation. However, as was suggested by Simone et al. [28], compressibility may increase turbulence intensity under certain conditions.

1.1 Rapid distortion theory

Inviscid rapid-distortion theory (RDT) [2] has long been used to study important linear aspects of turbulence physics. Insofar as incompressible flows are concerned, RDT has provided valuable insight into the rapid pressure-strain redistribution process which has led to important improvements in closure modeling (see reviews by [12,27] and references therein). In particular, RDT has played a significant role in improving our understanding of the effects of system rotation [7], stratification [6] and mean-flow unsteadiness [10] on turbulence. Analysis of compressible flows using RDT has been more recent—[4,7,8,28] and [19]. A brief review of the work performed to date in RDT of compressible homogeneous turbulence can be found in the recent work of Yu and Girimaji [30]. To date, application of RDT has been limited mostly to isentropic compressible turbulence evolving under the influence of specific forms of mean velocity gradients. The restriction to these special mean velocity gradients arises from the fact that homogeneity conditions are more restrictive in compressible turbulence. Recently, Yu and Girimaji [30] developed the formalism required to extend RDT of ideal-gas compressible turbulence to arbitrary mean velocity gradients. The governing equations consist of mass, momentum, energy equations supplemented by the state equation of ideal gas. This permits a more complete investigation of the role of pressure including flow-thermodynamics coupling. Some important aspects of ideal-gas turbulence subject to homogeneous shear have been investigated using RDT by Livescu and Madnia [19]. The small-scale structure and degree of anisotropy of velocity derivative moments have been carefully examined in this work. Simone et al. [28] perform a close examination of the effect of distortion Mach number (based on an integral lengthscale) on turbulent kinetic energy evolution. They find that at large Mach numbers, kinetic energy grows more rapidly than in incompressible turbulence at early times and markedly more slowly at later times.

An important predecessor to the present effort is the work of Livescu et al. [18]. In that paper, the evolution of compressible turbulence subject to shear and heat release is investigated and important conclusions are drawn. The authors demonstrate the complex interplay between compressibility, mean shear and heat release effects on turbulence. In our work, to gain further clarity, we investigate the linear and non-linear aspects of flow-thermodynamics interactions separately. Mean shear affects the large-scale linear interactions more profoundly than it does the small-scale non-linear interactions. These linear interactions are amenable to inviscid RDT investigation and is the subject of this paper. In many problems of interest to the current study (turbulent mixing/combustion, viscous boundary layer heating in hypersonic flows, etc.), heat release occurs in the small scales and has its most critical influence on non-linear interactions. To understand the non-linear flow-thermodynamic interactions with heat release, we examine decaying, anisotropic compressible turbulence with imposed temperature fluctuations. The results from that study are presented in the companion

paper, Lee and Girimaji [17]. The goal of this study is to investigate the compressibility effects in rapidly distorted homogeneous shear turbulence over a wide range of gradient Mach numbers and clearly characterize flow-thermodynamics interactions. Linear stability analyses have been reasonably successful in capturing important aspects of stabilizing physics in supersonic flows (e.g., [13]). Thus motivated, we will use the linear rapid distortion theory (RDT) to further our understanding of compressible turbulent shear flows.

Focus of current work. We perform ideal-gas compressible RDT analysis of initially isotropic turbulence subject to homogeneous shear to: (i) characterize the behavior of flow and thermodynamic statistics in various gradient Mach number regimes; and (ii) establish the nature of flow-thermodynamics interactions in the context of the changing character of pressure in the different regimes. For this investigation we use the RDT equations developed in [16,30] and employ isotropic incompressible initial field.

This paper is based on the M.S. thesis of Lavin [16]. For many of the detailed discussions, the reader is referred to the thesis. The remainder of this paper is organized as follows. Section 2 briefly discusses the governing equations in the rapid distortion limit. Numerical implementation issues are also discussed briefly. Results and analysis are presented in Sect. 3. Section 4 provides a brief summary of the important findings and concludes the paper.

2 Reynolds-averaged rapid distortion theory

The first step in deriving compressible RDT fluctuating-field equations is choosing the type of averaging to be employed. While Favre-averaging offers many physical advantages, the equations governing the evolution of fluctuations have been found to be very complicated. In this paper, we will employ the simpler Reynolds averaging as has been done in all preceding RDT works. The ensuing equations are called R-RDT equations, and details of their derivation can be found in [30]. In this section, we present only the salient features of the derivation and also briefly discus the numerical implementation.

2.1 RDT equations

We start with the conservation equations of mass, momentum and energy for an inviscid calorically perfect compressible medium:

$$\frac{\partial \rho}{\partial t} + U_k \frac{\partial \rho}{\partial x_k} = -\rho \frac{\partial U_k}{\partial x_k}; \tag{1}$$

$$\frac{\partial U_i}{\partial t} + U_k \frac{\partial U_i}{\partial x_k} = -\frac{1}{\rho} \frac{\partial p}{\partial x_i}; \tag{2}$$

$$\frac{\partial T}{\partial t} + U_k \frac{\partial T}{\partial x_k} = -T(\gamma - 1) \frac{\partial U_i}{\partial x_i} \tag{3}$$

where U_i, p, ρ and T represent velocity, pressure, density and temperature, and γ denotes ratio of specific heats. The symbols x_i and t represent spatial coordinates and time. Note that the following caloric equation of state has been used to express energy Eq. (3) in terms of temperature:

$$E = c_v T \tag{4}$$

where E and c_v are specific internal energy and specific heat at constant volume. For a perfect gas, the three thermodynamic variables are related through the state equation:

$$p = \rho R T \tag{5}$$

where R is gas constant.

The instantaneous values of velocity, pressure, density and temperature are decomposed into Reynolds-average (denoted by $(\bar{\cdot})$ or $\langle . \rangle$) and fluctuating (denoted by $(.'')$) components. We restrict our focus to homogeneous shear turbulence so that the gradients of mean thermodynamic properties are zero in addition to the mean velocity gradient being spatially uniform and temporally invariant.

2.1.1 Mean equations and parameters

We consider homogeneous shear of strength S:

$$\frac{\partial \overline{U}_i}{\partial x_j} = \begin{pmatrix} 0 & S & 0 \\ 0 & 0 & 0 \\ 0 & 0 & 0 \end{pmatrix}. \tag{6}$$

Under the influence of such a mean velocity field, mean density does not evolve in time:

$$\frac{\partial \overline{\rho}}{\partial t} = -\overline{\rho}\frac{\partial \overline{U_k}}{\partial x_k} = 0. \tag{7}$$

The governing equation of mean temperature ($\overline{T}$) can be derived by averaging the instantaneous energy Eq. (3):

$$\frac{\overline{\mathrm{d}T}}{\mathrm{d}t} = -\overline{u_j^{'}\frac{\partial T^{'}}{\partial x_j}} - (\gamma - 1)\overline{T^{'}\frac{\partial u_j^{'}}{\partial x_j}}. \tag{8}$$

Sound speed, a, is related to mean temperature as follows:

$$a = \sqrt{\gamma R \overline{T}}. \tag{9}$$

In DNS studies of homogeneous shear [25], a gradient Mach number based on an integral lengthscale has been recognized as the relevant parameter:

$$M_g = \frac{SL}{a}, \tag{10}$$

where S is the mean velocity gradient ($S \equiv \frac{\partial V_1}{\partial x_2}$) and L is an integral length-scale. However in an RDT analysis, the relevant lengthscale is one that is characteristic of the wavenumbers under consideration. Since this lengthscale is inverse of the magnitude of wavenumber, in this work we define gradient Mach number as:

$$M_g = \frac{S}{a\,|\kappa|}, \tag{11}$$

where $|\kappa|$ represents a norm of the wavenumbers under consideration. This gradient Mach number (11) is a measure of the relative significance of pressure effects to inertial effects in the velocity amplitude equation of a characteristic RDT mode.

2.1.2 Fluctuating flow equations

As stated in the introduction, two of the principal objectives of this work are to characterize the behavior of various turbulence statistics at various stages of evolution and explain the observed behavior in terms of the action of pressure during the different phases. For this we will need to develop equations for various turbulence statistics such as $\overline{u_i' u_j'}$, $\overline{T'T'}$, etc. In deriving the fluctuating field equations, as per classic RDT methodology, we disregard all terms that are non-linear in fluctuations. Thus the rapid distortion equations for fluctuating fields can be written as [16,30]:

$$\frac{\partial \rho'}{\partial t} + \overline{U}_k \frac{\partial \rho'}{\partial x_k} = -\overline{\rho}\frac{\partial u_k'}{\partial x_k}; \tag{12}$$

$$\frac{\partial u_i'}{\partial t} + \overline{U}_k \frac{\partial u_i'}{\partial x_k} = -u_k' \frac{\partial \overline{U}_i}{\partial x_k} - R\frac{\partial T'}{\partial x_i} - \frac{R\overline{T}}{\overline{\rho}}\frac{\partial \rho'}{\partial x_i}; \tag{13}$$

$$\frac{\partial T'}{\partial t} + \overline{U}_k \frac{\partial T'}{\partial x_k} = -(\gamma - 1)\overline{T}\frac{\partial u_k'}{\partial x_k}. \tag{14}$$

Again, as per common practice, to solve the linear RDT fluctuating field ODEs, we transform the equations to Fourier space (e.g., [23]). The fluctuating variables in (12)–(14) are expressed in terms of their Fourier components, and their evolution equations can be written as:

$$\frac{\mathrm{d}\widehat{\rho}}{\mathrm{d}t} = -i\overline{\rho}\kappa_k\widehat{u}_k; \tag{15}$$

$$\frac{\mathrm{d}\widehat{u}_i}{\mathrm{d}t} = -\widehat{u}_k\frac{\partial\overline{U}_i}{\partial x_k} - i(R\widehat{T} + \frac{R\overline{T}}{\overline{\rho}}\widehat{\rho})\kappa_i; \tag{16}$$

$$\frac{\mathrm{d}\widehat{T}}{\mathrm{d}t} = -i(\gamma-1)\overline{T}\kappa_k\widehat{u}_k. \tag{17}$$

where i is the imaginary unit equal to $\sqrt{-1}$. The wavenumber vector evolves as [23]:

$$\frac{\mathrm{d}\kappa_i}{\mathrm{d}t} + \kappa_k\frac{\partial\overline{U}_k}{\partial x_i} = 0. \tag{18}$$

Equations (15)–(18) can be directly solved and then used to construct the required covariances of fluctuating terms. Instead, we follow the particle representation method (PRM) approach recommended by Kassinos and Reynolds [14]. The PRM strategy significantly reduces the statistical error encountered in computing statistics from individual wave-vector realizations. Accordingly, we define various Fourier covariances, which can be interpreted as conditional moment for a given wavenumber [23]. Detailed description of the evolution equations of these co-variances is available in [16,30]. The equation set comprises of 26 linear ODEs.

Important caveats: Before proceeding with the results and analyses, it is important to understand the limitations of the RDT methodology in general. The forms of the basic conservation and state equations used are valid only for continuum fluid that is close to thermodynamic equilibrium. Rarefied gas and high-temperature real-gas effects that influence many hypersonic flows are not accounted for in this study. Only the so-called 'hydrodynamic' high Mach number effects are considered. The omission of non-linear terms in the conservation equations further restricts the generalization of RDT findings to turbulent flows. However, RDT is the best tool to develop fundamental understanding of the so-called 'rapid' pressure effects. Rapid pressure-strain correlation is an important turbulence process that is primarily responsible for any stabilizing/destabilizing influence of compressibility. Overall, in agreement with [19] and [28], we suggest that the current RDT method is well suited for investigating linear turbulence physics for a wide range of gradient Mach numbers.

2.2 Numerical implementation and verification

In this work we employ a high-fidelity fourth-order Runge-Kutta scheme to solve the ODEs. The scheme has been previously validated in [9] and [30]. The initial velocity field is incompressible and statistically isotropic. Initial conditions for the wavenumber vector and 25 covariances are specified in Fourier space. The details can be found in [9] and [30], and we will only present the salient points here. The wavenumber $\boldsymbol{\kappa}(t=0)$ and corresponding velocity covariance $R_{ij}(t=0)$ are first chosen: wavevectors are distributed uniformly on a unit sphere to render a statistically isotropic initial field. To ensure initial incompressibility, velocity vectors for each wavevector are chosen such that they are normal to the respective wavevector. Density is set so that $\overline{\rho} = 1.0$, while initial mean temperature is set to 300 K. Finally, the RMS (root mean square) of density and temperature fluctuations are specified as percentages of the mean density and temperature, respectively. In our study, it is found that the results are independent of the initial temperature fluctuations so long as the intensity of the fluctuations is less than 3%. Discernible differences are seen only beyond 5%. All results presented here are for initial temperature intensity less than 3% and no density fluctuations. The pressure fluctuations are determined from temperature fluctuations. The initial pressure fluctuations do not necessarily satisfy the Poisson equation. This is justified by the fact that pressure equilibration takes a few acoustic times and in high-speed shear flows any induced velocity perturbations will not be correlated to pressure perturbations. The initial length scale is taken to be unity: $l_0 = 1/|\kappa(t=0)| = 1$. The mean flow of interest is the steady homogeneous shear as defined in (6). The magnitude of S, the sound speed and initial length-scale of perturbation determine the initial gradient Mach number (11), which is the chief parameter of the present study.

2.2.1 Parameter range

We perform RDT computations with different gradient Mach numbers ranging from $M_{g0} \equiv M_g(t=0) = 0.01$, which represents the incompressible limit to $M_{g0} = 2{,}880$, which represents the so-called pressure-release or Burgers limit [28]. In the Burgers limit, the timescale of pressure is very long compared to that of shear. Although, not of practical utility, computations of $M_{g0} = 2{,}880$ are used to validate the numerical implementation by comparison against Burgers pressure-released limit analytical results [28]. Other relevant parameters that are not considered in this study include change in turbulent Mach number, initial solenoidal-dilatational composition ratio and initial intensities of thermodynamic fluctuations.

During the course of a simulation, the gradient Mach number changes as the wavenumber evolves according to Eq. (18). Using this equation we can write

$$\begin{aligned} \frac{\mathrm{d}\kappa_1(t)}{\mathrm{d}t} &= 0; \quad \text{implying} \quad \kappa_1(t) = \kappa_1(0); \\ \frac{\mathrm{d}\kappa_2(t)}{dt} &= -\kappa_1 \frac{\partial U_1}{\partial x_2}; \quad \text{implying} \quad \kappa_2(t) = \kappa_2(0) - \kappa_1(0) St; \\ \frac{\mathrm{d}\kappa_3(t)}{\mathrm{d}t} &= 0; \quad \text{implying} \quad \kappa_3(t) = \kappa_3(0). \end{aligned} \tag{19}$$

From these equations, it is easy to deduce that

$$\kappa^2(t) \sim \kappa^2(0) \left(1 + \frac{S^2 t^2}{3}\right). \tag{20}$$

Since the relevant lengthscale is inverse of the magnitude of wavenumber, we can estimate the lengthscale of characteristic turbulence fluctuations at given time t as

$$l(t) = 1/|\kappa| \sim \sqrt{\frac{3}{3 + S^2 t^2}}. \tag{21}$$

where $\kappa^2(0) \sim 1$. We can now estimate the gradient Mach number (11) as a function of time:

$$M_g(t) \sim \frac{Sl(t)}{a_0} = M_{g0} \sqrt{\frac{3}{3 + S^2 t^2}} \sim \sqrt{3} \frac{M_{g0}}{St}. \tag{22}$$

Thus, in all cases, the gradient Mach number decreases with time. Initially incompressible flows will continue to remain incompressible at all times. Given adequate time, even very high M_{g0} flows will ultimately evolve into a low Mach-number regime.

2.2.2 Spectral-grid and time-step resolution study

We now establish the adequacy of the Fourier space (number of wave-vector modes) and time discretization employed in this study. To examine the dependence of the RDT results on spectral discretization, we present results from three isotropically distributed sets of wave-vectors of different populations (N): 6,079, 12,000 and 16,000. It is very important to recognize that the solenoidal and dilatational portions of the velocity field have completely different resolution requirements. As a result, we examine not only the total kinetic energy behavior as a function of resolution, but also the individual characteristics of the solenoidal (vortical) and dilatational (acoustic) fields. For the homogeneous shear flow configuration employed in this study, the fluctuating velocity in the streamwise (1-) direction is nearly purely solenoidal. The fluctuating velocity in the stream-normal direction (2-) is almost entirely dilatational or acoustic. It is important to recall that the fluctuations in the stream-normal direction nearly vanish in low speed shear flows due to the incompressibility constraint. We investigate the results for initial gradient Mach number of unity as this features the maximum level of acoustic fluctuations.

In Figs. 1, 2, 3 and 4 we present time evolution of kinetic energy, $\overline{u_1 u_1}$ and $\overline{u_2 u_2}$ with the three set of wave-vectors. It is immediately evident that the total kinetic energy evolution exhibits some small amplitude oscillations at late times and the three computations exhibit some disparity. To gain further insight, we examine the solenoidal and dilatational energies individually next. Expectedly, the solenoidal part (Fig. 4—$\overline{u_1 u_1}$)

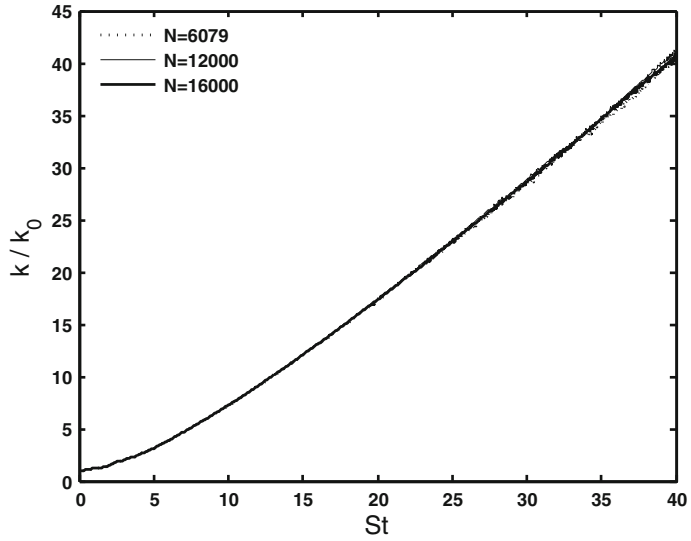

Fig. 1 Evolution of kinetic energy, k ($= \frac{\overline{u_i u_i}}{2}$) in simulations with different Fourier grids. N denotes total number of wave-vectors of a spectral grid and k_0 is initial kinetic energy. Initial gradient Mach number is unity

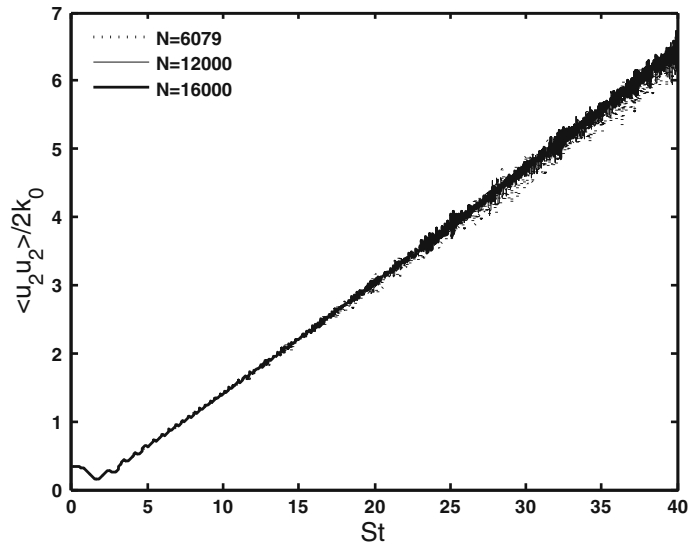

Fig. 2 Evolution of $\overline{u_2 u_2}$. Initial gradient Mach number is unity

exhibits no oscillations and the computations of the three computations generally agree well to within statistical error. This leads to the inference that solenoidal field generally needs much smaller level of resolution and this has been demonstrated in the incompressible RDT works of Girimaji et al. [9] and Mishra and Girimaji [21]. In this compressible RDT study, the acoustic part of the velocity field $\overline{u_2 u_2}$ exhibits oscillations with generally small but distinct difference between the computations (Figs. 2 and 3). The frequency of oscillation does not change with different resolutions, but the amplitude decreases marginally with superior resolution. However, there is clearly no systematic change in the overall result with change in the wave-vector population from 6,079 to 16,000. The disagreement between the various resolutions is smaller at higher or smaller gradient Mach number computations [16].

Now we present an explanation for the observed behavior of acoustic oscillations at the different resolutions. The persistence of oscillations in RDT calculations seen at late times have been observed and explained in previous studies [28] as well. Inherently, each individual wavenumber simulated exhibits acoustic high-frequency oscillations especially at late times as the acoustic timescale becomes much smaller than the solenoidal timescale. The collective behavior of the RDT ensemble depends upon the number of energetic contributing

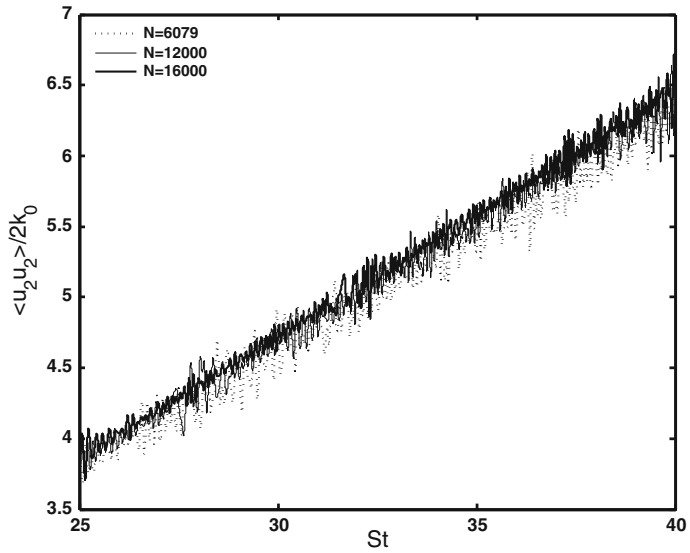

Fig. 3 Evolution of $\overline{u_2 u_2}$ (magnified view). Initial gradient Mach number is unity

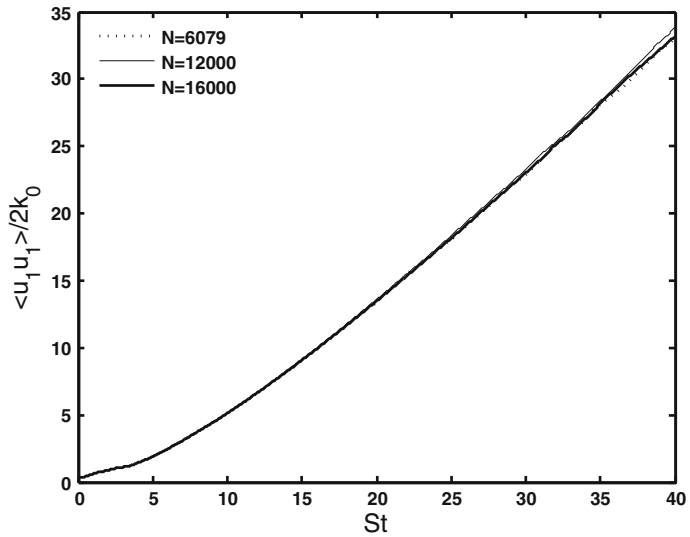

Fig. 4 Evolution of $\overline{u_1 u_1}$. Initial gradient Mach number is unity

modes. At early times, all modes are nearly equally energetic due to the initial specifications. Therefore, the contributing statistical sample size is large and the acoustic oscillations of the various modes cancel out to yield smooth evolution of statistics. With passage of time different modes evolve at different rates. Soon fewer and fewer high energy modes contribute to the overall statistics. Due to shrinking sample size, the statistics begin to mirror the oscillations of the few contributing modes. Irrespective of the initial number of wave-vectors, at sufficiently long times, the statistics will exhibit oscillatory evolution due to diminishing number of contributing wave-vectors. For the purposes of the present study, it is deemed that an initial population of 6,079 wave-vectors provides the requisite statistical resolution over the duration of the simulation. Higher number of wave-vectors may yield slightly smoother evolution of the statistics at late times without altering the physical inferences.

To establish the adequacy of the temporal discretization, we perform computations with a smaller time-step size and compare the results with the original set of computations. Figure 5 compares the evolution of dilatational kinetic energy for a representative gradient Mach number (similar study was performed with different initial gradient Mach number as well) in simulations with two different time-step sizes. The agreement is

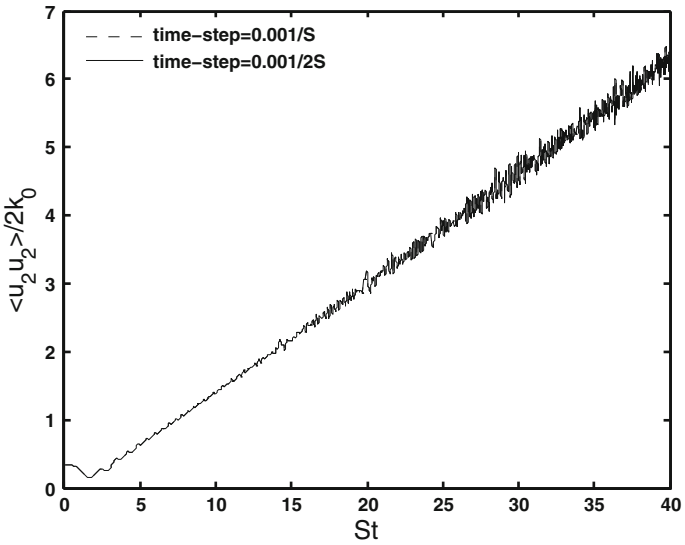

Fig. 5 Evolution of $\overline{u_2 u_2}$ in simulations employing different time-step sizes. Initial gradient Mach number is unity and the total number of wave-vectors is 6,079 for both simulations

excellent. Similar agreement is seen in other quantities as well. The exact agreement between the two cases clearly demonstrates that original time step size is adequate.

In [30] it was shown that the current RDT methodology recovers published [23] incompressible RDT kinetic energy and Reynolds stress anisotropy data precisely. At the other extreme, for very high gradient Mach number, Yu & Girimaji [30] show that the current method produces results that match the exact pressure-release analytical solution given in [28]. At intermediate Mach numbers, it must be pointed out that the velocity field results are consistent with that of isentropic RDT of [28]. Thus, the RDT numerical implementation employed in this paper produces results that are fairly insensitive to time-step and Fourier-grid size and yields physically correct behavior at the asymptotic limits of zero and very large (2,880) Mach numbers.

2.3 RDT validation

To demonstrate the relevance of inviscid linear theory to physical intermediate Mach number turbulence, we compare our RDT results against homogeneous-shear direct numerical simulation (DNS) data of [28]. As RDT neglects non-linear interactions and viscous effects, we cannot expect a precise agreement with DNS. We only aim for qualitative agreement that captures all the key physical trends. We compare the evolution of RDT and DNS solenoidal anisotropy component b_{12}^s over a limited Mach number range in Fig. 6. Note that very high Mach number simulations that are easily performed with RDT cannot be calculated with DNS due to extremely large computational costs. Although there are distinct differences between RDT and DNS attributable to non-linear effects, the general trends with increasing Mach number are very similar. The transient-peak and asymptotic b_{12}^s values in the two cases are quite close. The dilatational anisotropy component b_{12}^d from DNS and RDT are compared in Fig. 7. DNS indicates that the dilatational shear stress is quite insensitive to Mach number and RDT captures this trend very well. In fact, at higher Mach numbers, the agreement between RDT and DNS is quite good at all times. This is due to the fact that linearization is more justified at larger gradient Mach numbers than at smaller values. Livescu et al. [19] show more comparisons between RDT and DNS that further justify the use of RDT as an analytical tool to investigate compressible turbulence phenomena.

3 Results and analysis

In keeping with the objectives of the study, this section is sub-divided into three parts: (i) characterization of velocity fluctuations; (ii) characterization of thermodynamic fluctuations; and (iii) investigation of flow-thermodynamic interactions.

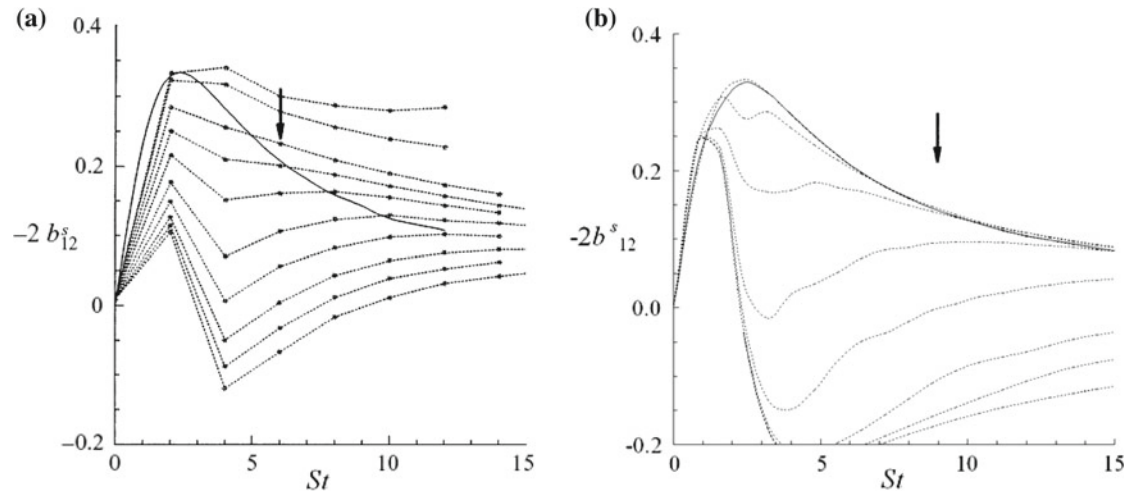

Fig. 6 Solenoidal b_{12} anisotropy component of initially-incompressible homogeneous turbulence in pure shear at various Mach numbers (*arrows* indicate direction of increasing Mach number). *Solid line* represents the incompressible limit. Plots are shown for **a** DNS [28] (reprinted with permission from Cambridge University Press, Copyright [1997]) and **b** R-RDT

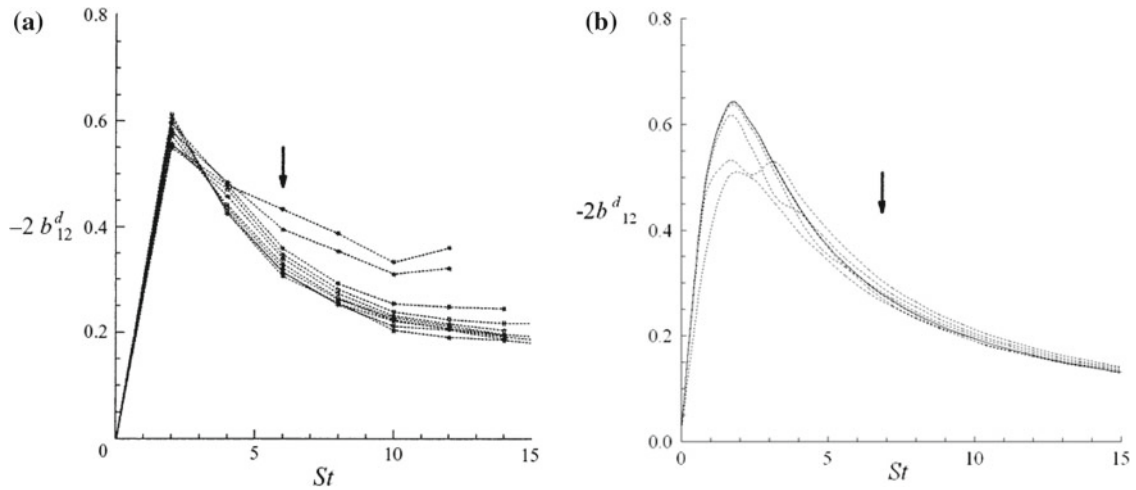

Fig. 7 Dilatational b_{12} anisotropy component of initially-incompressible homogeneous turbulence in pure shear at various Mach numbers (*arrows* indicate direction of increasing Mach number). *Solid line* represents the incompressible limit. Plots are shown for **a** DNS [28] (reprinted with permission from Cambridge University Press, Copyright [1997]) and **b** R-RDT

3.1 Characterization of velocity fluctuations

We first consider the evolution of kinetic energy. In the incompressible rapid distortion limit, turbulence behaves like an elastic phenomenon and its evolution depends on total deformation (St) rather than deformation rate (S) itself. At a given value of St, turbulence experiences the same mean deformation irrespective of the gradient Mach number. Further, it can be shown that incompressible RDT turbulence evolution is independent of S when considered in normalized time St. Therefore, it is common practice to consider incompressible turbulence evolution in St units. Following [28], we first show the kinetic energy evolution of compressible turbulence in St time units in Fig. 8 for a range of Mach numbers. Also included for comparison is the pressure-release (Burgers limit) analytical solution of [28]. Most evident is the fact that for a given total deformation (St) the kinetic energy is not a monotonic function of M_{g0}. Temporal evolution of the low Mach number cases ($M_{go} \leq 0.7$) is very similar to that of incompressible turbulence. The intermediate Mach number cases ($1 \leq M_{g0} \leq 5$) grow distinctly more slowly than the incompressible cases. High Mach number cases ($M_{g0} > 5$) exhibit a more complex behavior. At early times the kinetic energy grows very rapidly as in Burgers turbulence. Then, at some intermediate time, which depends on the initial Mach number, the growth rate slows down almost going

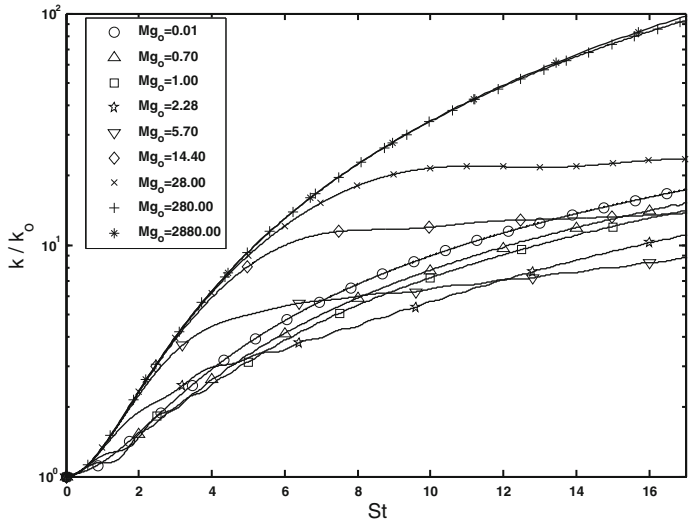

Fig. 8 Evolution of normalized turbulent kinetic energy with solenoidal initial conditions in shear time. Note that Burgers RDT evolution of kinetic energy ($\frac{k}{k_0} = 1 + \frac{(st)^2}{3}$ [28]) overlaps the case $Mg_0 = 2{,}880$ over the displayed range of shear time

to zero. At later St times, the kinetic energy is distinctly smaller than that of incompressible cases at the same level of deformation. Simone et al. [28] and Sarkar et al. [25] identify this slowdown in kinetic energy growth at intermediate and high Mach numbers as the stabilizing influence of compressibility.

Unlike incompressible turbulence, it is easy to verify that compressible RDT equations are not invariant to S in strain-normalized time St. Therefore, it may be instructive to examine the kinetic energy growth in other timescales. Clearly, acoustic timescale should be important in compressible turbulence. In Fig. 9, evolution of turbulent kinetic energy is presented in acoustic (ta_0/l_0) time units. Since the initial acoustic velocity and lengthscale are identical for all cases, the observed behavior can be regarded as real-time evolution. This scaling of time presents a vastly different and perhaps a clearer picture of the time evolution. The kinetic energy of the low Mach number ($M_{g0} < 0.7$) cases show no significant growth during the first several acoustic time units. When growth does start, it is qualitatively same in all low-M_{g0} cases. In the high Mach-number cases considered ($M_{g0} > 5$), turbulence evolution exhibits three distinct stages: early period of rapid k growth followed by duration where k is nearly a constant and a final period increased growth rate. The intermediate Mach-number cases exhibit only two stages: initial period of slow or no growth followed by more rapid growth. Significantly, asymptotic growth rate in all cases appear quite similar. Despite the variable growth rates of intermediate

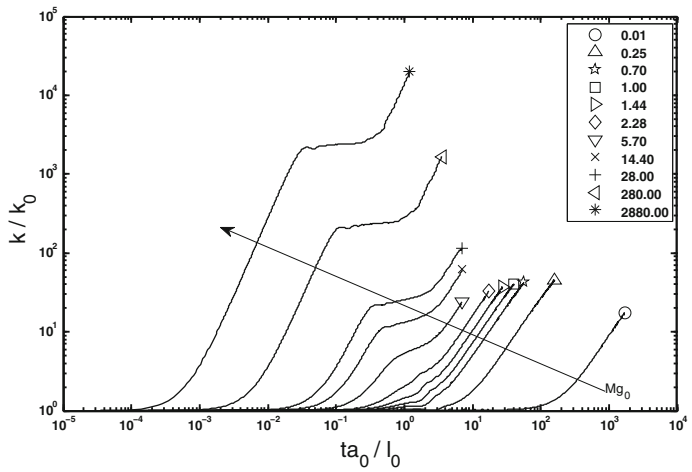

Fig. 9 Kinetic energy evolution versus acoustic time (ta_0/l_0) with solenoidal initial conditions, where a_0 and l_0 represent initial sound speed and length scale

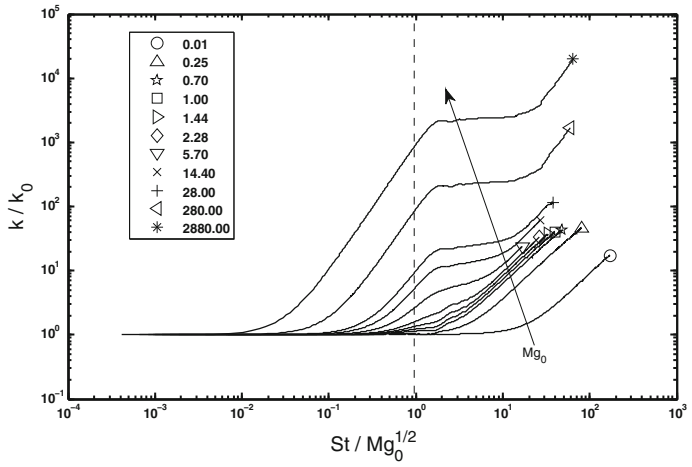

Fig. 10 Kinetic energy versus normalized time

and high Mach number cases, for a given elapsed time, kinetic energy content increases monotonically with Mach number. Clearly, incompressible and Burgers real-time evolution represent the two extreme limits of homogeneous compressible shear flow behavior. Interestingly, the final-stage growth of all intermediate and high M_{g0} appear to set in at about one acoustic time unit: $0.5 \leq \frac{ta_0}{l_0} \leq 3$. It is significant to note that one acoustic time unit ($t = l_0/a_0$) also corresponds to $St = M_{g0}$ and the time when the time-evolving gradient Mach number is unity $M_g(t) \approx 1$. This final stage of high M_{g0} cases is qualitatively similar to the asymptotic growth stage of low-M_{g0} cases.

We next plot kinetic energy growth in Fig. 10 in mixed (geometric mean) strain-acoustic time: $St/\sqrt{M_{g0}}$. Again, the three different stages of turbulence evolution are apparent. This scaling of time clearly demarcates the duration of the first stage of growth. It is apparent that the switch from the rapid-growth first stage to nearly zero-growth second stage happens at $St \sim \sqrt{M_{g0}}$ (dashed line in Fig. 10).

Regimes of turbulence Based on the kinetic energy evolution, we recognize—along the lines of [3,16,20,24,29] – that three regimes of compressible turbulence behavior are possible. The demarcations between these regimes are: the first regime occurs in the time interval $0 < St \leq 2\sqrt{M_{g0}}$; the time interval of the second stage is $2\sqrt{M_{g0}} \leq St \leq O(M_{g0})$; and the final regime of behavior occurs at all later times: $St > O(M_{g0})$. The observations provide a basis for classifying the regimes as follows.

1. In the first regime, as evident from Fig. 8, the evolution is close to that of Burgers turbulence due to the fact that pressure effects are negligible at the high Mach numbers. Thus, it is reasonable to call this early period pressure-release (PR) regime.
2. With passage of time, the Mach number decreases as per (22), and at very large times ($St > M_{g0}$) the Mach number falls below unity. It is reasonable to call this stage the sub-sonic or low-Mach number (LM) regime.
3. Between PR and LM regimes lies the stage wherein the wave character of pressure manifests. Hence, we call this the wave-character (WC) regime.

We will now examine the behavior of individual velocity correlations in the three regimes. Most of the subsequent discussion employs mixed shear-acoustic time normalization as that evidently provides the clearest demarcation between the various regimes.

In Fig. 11 we present the evolution of the streamwise kinetic energy ($\overline{u_1u_1}$). The behavior seen in the figure is very similar to that of total kinetic energy exhibiting the three Mach number regimes. This should not be surprising as the streamwise fluctuations constitute a very high fraction of total, kinetic energy. The evolution of stream-normal kinetic energy ($\overline{u_2u_2}$) is plotted in Fig. 12. The overall magnitude is much lesser than that of $\overline{u_1u_1}$ as there is no direct production of this component. While three regimes of behavior are again evident, manner of evolution in each regimes is quite different from that of k and $\overline{u_1u_1}$. In the PR regime, $\overline{u_2u_2}$ is virtually a constant initially and dips slightly toward the end. The $\overline{u_2u_2}$ growth is oscillatory in the second and third stages: the net growth is slightly higher in WC regime than during the LM period. The oscillatory nature

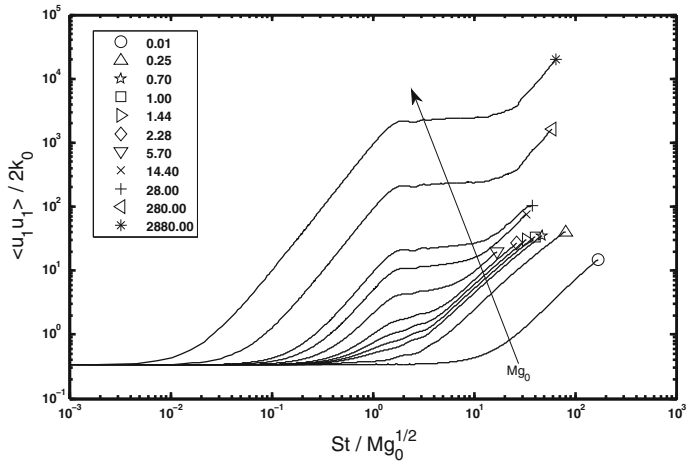

Fig. 11 Streamwise component ($\frac{\overline{u_1 u_1}}{2k_0}$) of turbulent kinetic energy versus normalized time

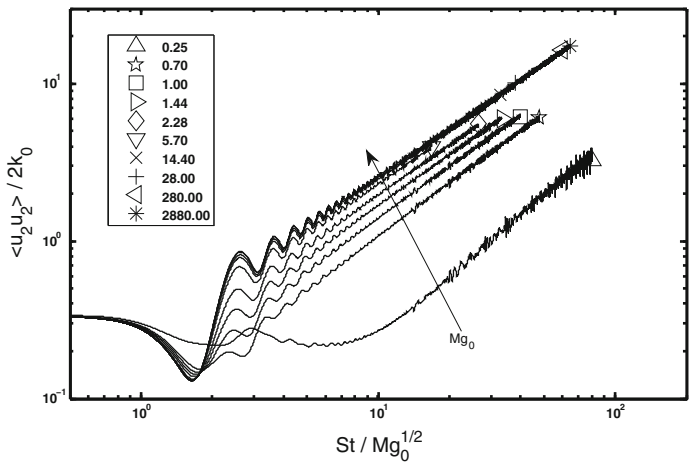

Fig. 12 Stream-normal ($\frac{\overline{u_2 u_2}}{2k_0}$) component of turbulent kinetic energy versus normalized time

is more pronounced in WC rather than LM stage. It is a simple matter to recognize that $\overline{u_2 u_2}/2$ represents dilatational kinetic energy. With κ_2 being the only significant component of wavevector at late times, any fluctuation with non-zero u_2 must be dilatational [19]. By the same token, the kinetic energy associated with u_1 and u_3 is most likely due to solenoidal or incompressible motion. The evolution of $\overline{u_3 u_3}$ for the various cases is shown in Fig. 13. This component is virtually unchanged from its initial value in the PR zone. During the WC period, this energy component grows. But the growth rate in the intermediate regime appears to be a function of initial Mach number. Smaller the initial Mach number, larger is the intermediate-regime growth rate. The growth rate reaches its peak in the LM regime. The evolution of shear-stress ($\overline{u_1 u_2}$) is shown in Fig. 14 in St time and in Fig. 15 in $St/\sqrt{Mg_0}$. The small Mach-number cases follow the incompressible behavior fairly closely. The higher Mach-number cases show a significant difference. During the PR period $\overline{u_1 u_2}$ is negative as in the incompressible case but the magnitude is larger. This results in larger turbulence production and higher levels of kinetic energy. The duration of PR regime increases with increasing initial Mach numbers. At later times (WC regime), $\overline{u_1 u_2}$ is oscillatory around a mean value of zero. Consequently, production vanishes explaining why the kinetic energy growth rate is nearly zero in the WC regime. With passage of more time, the amplitude of $\overline{u_1 u_2}$ significantly diminishes even as the oscillations fade away. Finally, during the LM period, the negative correlation between u_1 and u_2 is re-established as indicated by $\overline{u_1 u_2}$ values approaching that of incompressible turbulence.

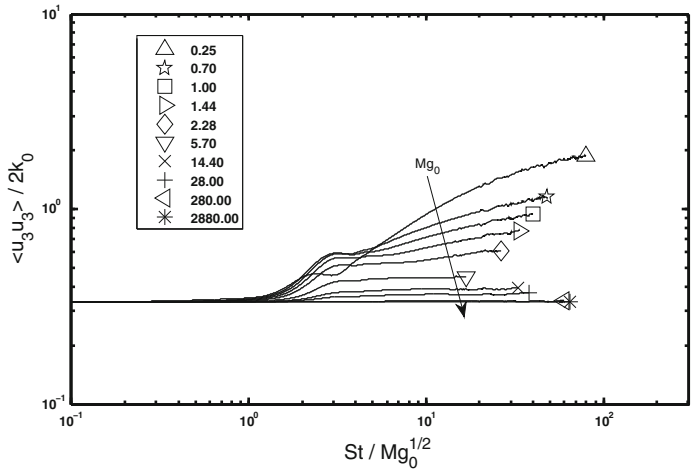

Fig. 13 Stream-transverse ($\frac{\overline{u_3 u_3}}{2k_o}$) component of turbulent kinetic energy versus normalized time

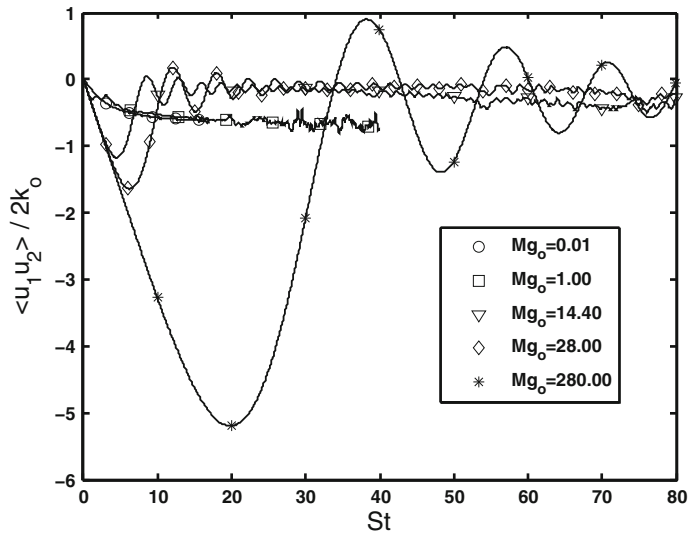

Fig. 14 Normalized Reynolds shear stress ($\frac{\overline{u_1 u_2}}{2k_o}$) in shear time ($St$)

3.2 Characterization of thermodynamic fluctuations

All of the previous works have focused on kinetic energy and by virtue of employing perfect-gas state equation in this work, we present an accurate account of the internal/total energies and thermodynamic (density and temperature) fluctuations as well.

3.2.1 Internal energy

The evolution of change in internal energy, ΔE ($=c_v(\overline{T} - \overline{T}_0)$) as a function of Mach number is shown in Fig. 16. Again, the three-regime behavior is evident. In the PR regime, there is virtually no change in energy. In the WC zone, there is a strong growth in internal energy even as oscillations are evident. Finally, the oscillations fade away, followed by monotonic growth in the LM regime. Internal energy evolution bears a strong resemblance to that of $\overline{u_2 u_2}$ in all the regimes. In Fig. 17, the evolutions of internal energy and $\frac{\overline{u_2 u_2}}{2}$ are compared for a few select cases. Strikingly, the two are nearly identical (even though the oscillations are out of phase) in WC and LM regimes. This observation strongly suggests equipartition of energy between dilatational turbulent kinetic energy and internal energy increase. This equipartition is seen in all of the computed cases.

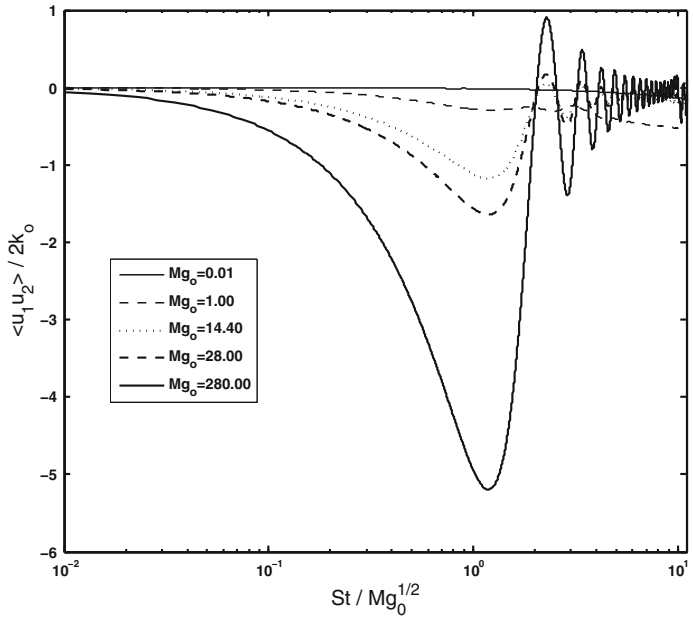

Fig. 15 Normalized Reynolds shear stress ($\frac{\overline{u_1 u_2}}{2k_o}$) versus normalized time

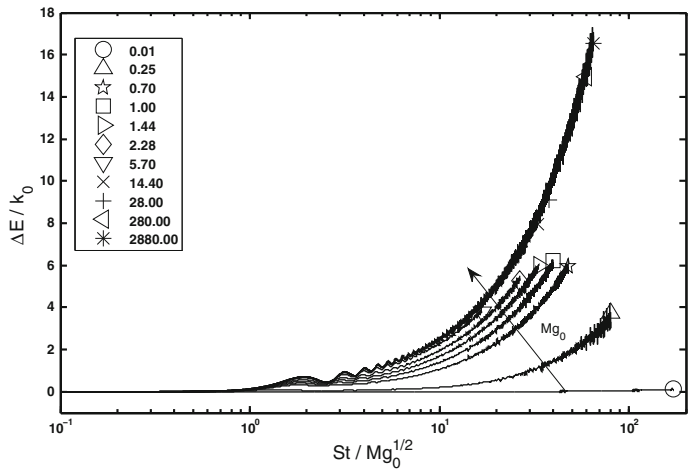

Fig. 16 Change in internal energy versus normalized time

3.2.2 Density and temperature fluctuations

The evolution of density and temperature fluctuations are given in Figs. 18 and 19 respectively. The density variance does not grow in the PR regime, experiences oscillatory growth during WC period followed by monotonic increase in the LM stage. Temperature evolution also shows a similar trend. Due to lack of coupling between thermodynamic and flow fields, the thermodynamic variables do not grow in the PR regime. In LM regime, they grow nearly linearly as dilatational and solenoidal fields evolve independently.

3.3 Flow-thermodynamic interactions

The thermodynamic state variables—density and temperature—appear explicitly in the Navier-Stokes equations and serve as the conduits for flow-thermodynamics interactions. In this work we examine the flow-thermodynamics interactions by focusing on the behavior of the pressure-strain correlation tensor (Π_{ij}) and its trace, pressure dilatation (Π_{kk}),

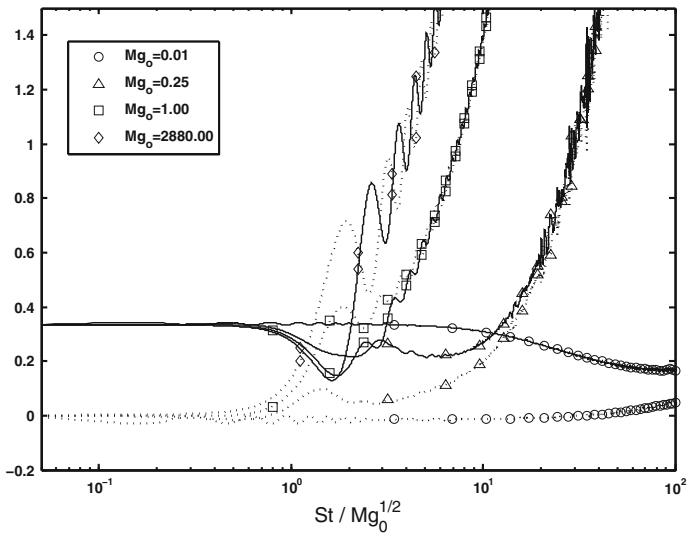

Fig. 17 Change in internal energy and growth of $\frac{\overline{u_2u_2}}{2}$ component of turbulent kinetic energy versus normalized time. *Solid curves*: $\frac{\overline{u_2u_2}}{2k_o}$. *Dotted curves*: $\frac{\Delta E}{k_o}$

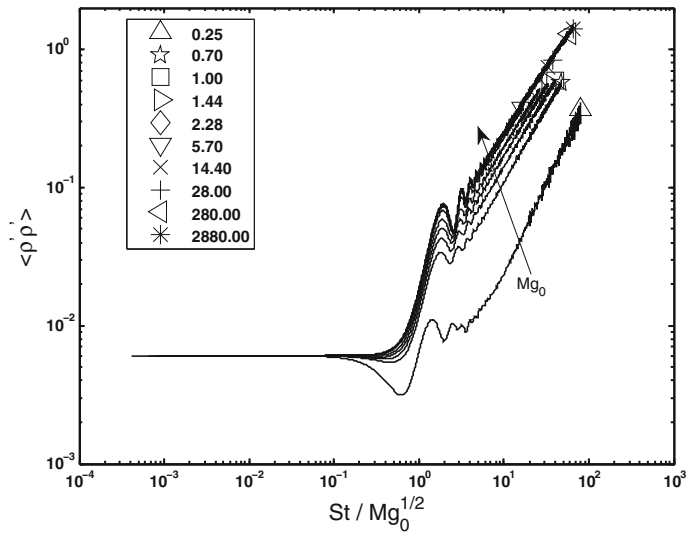

Fig. 18 Density fluctuation versus normalized time

$$\Pi_{ij} = \overline{\frac{p'}{2}\left(\frac{\partial u_i^{'}}{\partial x_j} + \frac{\partial u_j^{'}}{\partial x_i}\right)}. \tag{23}$$

Specifically, we examine how the redistributions among the various Reynolds stress components and that between kinetic and internal energy are affected by gradient Mach number.

In low gradient Mach number incompressible flows, density is constant and pressure is a Lagrange multiplier rather than a thermodynamic state variable. In this flow regime it has been well documented that pressure-strain correlation transfers energy from streamwise ($\overline{u_1u_1}$) and stream-normal ($\overline{u_2u_2}$) fluctuations to transverse ($\overline{u_3u_3}$) fluctuations. Correspondingly, pressure-strain tensor components Π_{11} and Π_{22} are negative and Π_{33} is positive. Finally, pressure-dilatation is negligible indicating that there is no transfer of energy from kinetic to internal form. These energy exchanges are schematically captured in Fig. 20.

As the gradient Mach number increases, pressure acquires thermodynamic significance and its evolution is now governed by the energy and state equations. Under these conditions, pressure attains wave-like character and consequently pressure-strain correlation evolution becomes highly oscillatory. First we examine

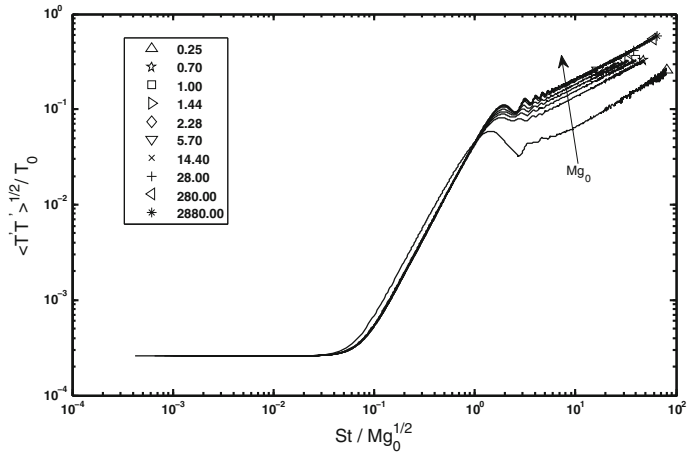

Fig. 19 Temperature fluctuation versus normalized time

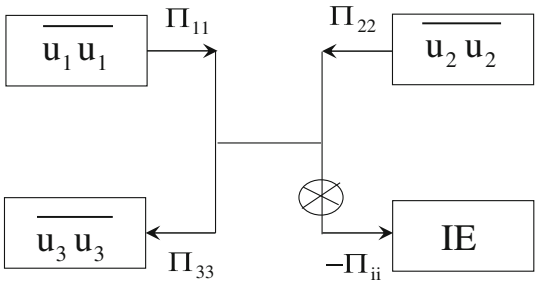

Fig. 20 Energy transfer in incompressible turbulence (IE implies mean internal energy, $IE = c_v \overline{T}$)

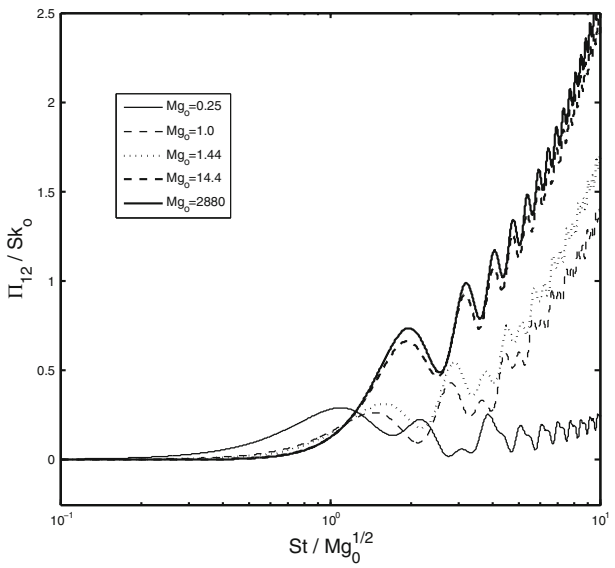

Fig. 21 Evolution of Π_{12} versus normalized time

the behavior of Π_{12} component in Fig. 21. As expected, Π_{12} does not evolve much in the early PR stage, because the flow field is dominated by inertial action and pressure has negligible role to play in this stage. In the WC regime, owing to the dominant wave nature of pressure, Π_{12} begins to evolve with oscillations that continue into the LM regime as well. However in the LM regime, a distinct near monotonic growth can be clearly observed. Moreover, we observe that at any given time instant ($\frac{St}{\sqrt{Mg_0}}$), strength of Π_{12} is higher in

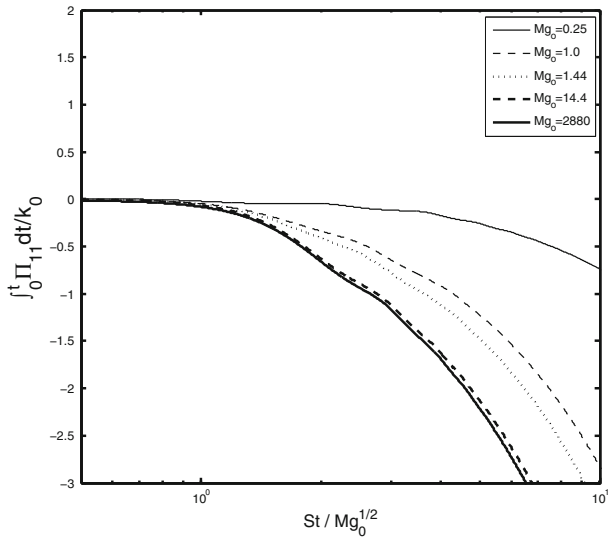

Fig. 22 Time-integrated Π_{11} ($\frac{1}{k_0}\int_0^t \Pi_{11}\mathrm{d}t$) versus normalized time

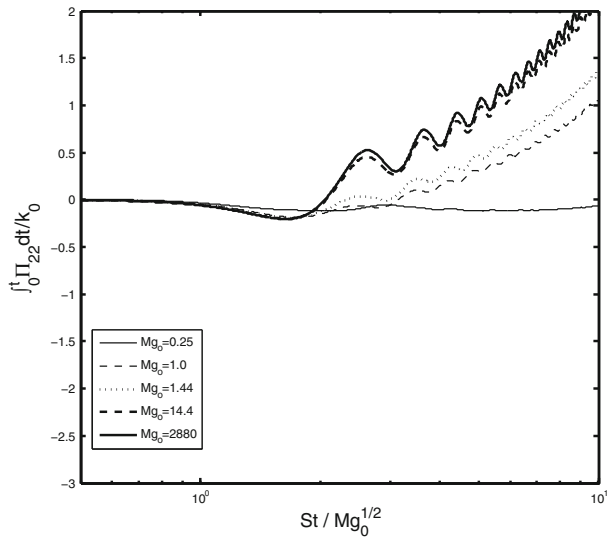

Fig. 23 Time-integrated Π_{22} ($\frac{1}{k_0}\int_0^t \Pi_{22}\mathrm{d}t$) versus normalized time

a simulation with higher initial gradient Mach number. All these trends observed in Fig. 21 are very similar to the trends earlier seen in the case of thermodynamic fluctuations: $\overline{T'T'}$ and $\overline{\rho'\rho'}$ (Figs. 18 and 19). Since the strength of pressure fluctuation is simply a linear combination of density and temperature fluctuations, we can conclude that the overall behaviour of Π_{12} correlation in various regimes of rapid-distortion is principally shaped by the behaviour of thermodynamic fluctuations.

Our results reveal that a direct examination of the normal pressure-strain tensor components is difficult as the oscillatory behavior obfuscates the overall energy transfer details. Instead, we investigate the evolution of the temporal integral of the normal pressure-strain tensor components. Such an approach is reasonable as the integral represents the net amount of transferred energy—recall that pressure-strain component is the transfer rate. In Figs. 22, 23, 24, 25, we present the evolution of the integral of the normal pressure-strain correlation tensor components and their sum—pressure dilatation. Again, in the beginning of the PR regime, all components are understandably small and the flow evolves impervious to the thermodynamic state variables. However toward the end of the PR regime ($1 < \frac{St}{\sqrt{Mg_0}} < 2$) pressure correlations become sizable and start influencing the turbulent fluctuations. As can be seen from the figures, during this stage, the integrals of Π_{11}, Π_{22}, Π_{ii} are

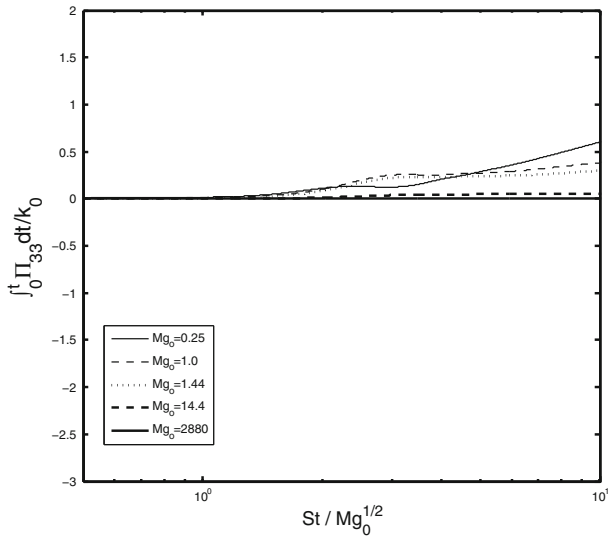

Fig. 24 Time-integrated Π_{33} ($\frac{1}{k_0}\int_0^t \Pi_{33}\mathrm{d}t$) versus normalized time

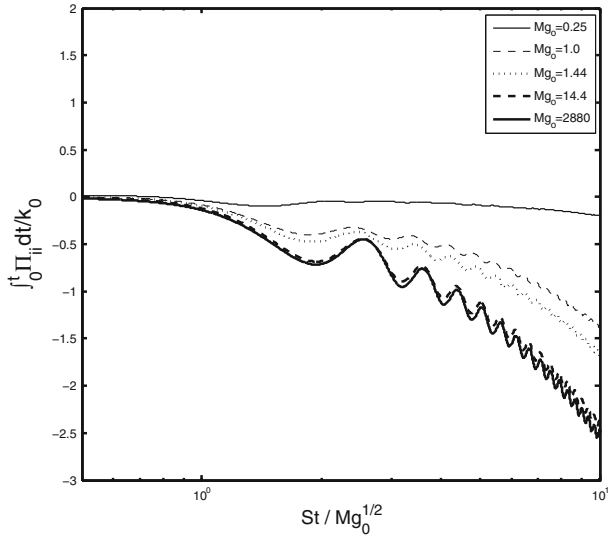

Fig. 25 Time-integrated Π_{ii} ($\frac{1}{k_0}\int_0^t \Pi_{ii}\mathrm{d}t$) versus normalized time

all negative and Π_{33} is positive. The inference is that energy is drawn from $\overline{u_1u_1}$ and $\overline{u_2u_2}$ components and deposited into internal energy and $\overline{u_3u_3}$. These energy exchanges are schematically captured in Fig. 26.

As turbulence evolution enters the WC stage ($\frac{St}{\sqrt{Mg_0}} \geq 2$), we see an important change in the energy exchange dynamics. The sign of the integral of Π_{22} changes to positive from negative, while those of Π_{11} and Π_{ii} continue to be negative during the WC and LM regimes. Further, Π_{33} becomes sizable and continues to grow. The corresponding energy transfer scenario is presented in Fig. 27. Pressure removes energy from the streamwise fluctuations and transfers it into internal energy and also into stream-normal and transverse velocity fluctuations. Furthermore, in a simulation with higher initial gradient Mach number, Π_{11}, Π_{22} and Π_{ii} get amplified indicating more transfer of energy from stream wise direction to stream-normal and to the internal mode of energy. However, the tendency of energy transfer to transverse direction ($\overline{u_3u_3}$) is monotonically suppressed as gradient Mach number increases. This is evident in Fig. 24.

We will now summarize and explain the observed behavior. In the early PR regime, flow-thermodynamics interactions are negligible as the flow inertia dominates over pressure effects. Toward the end of the PR regime, pressure fluctuations become important and begin to drive turbulence toward equipartition of energy

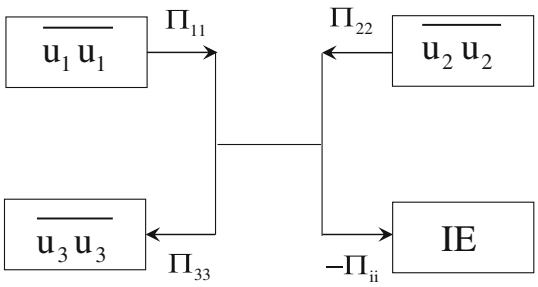

Fig. 26 Energy transfer in PR regime of compressible turbulence (IE implies mean internal energy, $IE = c_v\overline{T}$)

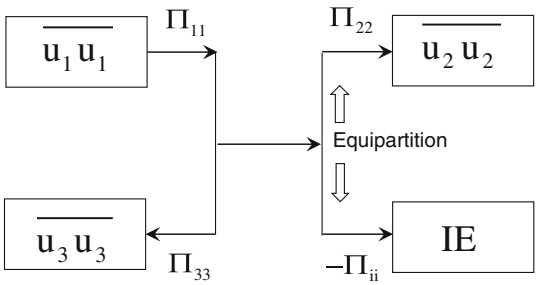

Fig. 27 Energy transfer in WC and LM regimes of compressible turbulence (IE implies mean internal energy, $IE = c_v\overline{T}$)

between the internal mode and dilatational component ($\overline{u_2 u_2}$). Since in the beginning of the of PR regime there is substantial disparity between $\overline{u_2 u_2}/2$ and internal energy (see Fig. 17, $\overline{u_2 u_2}/2 > \Delta E$), the immediate action of pressure is to: (a) lower $\overline{u_2 u_2}$ (via Π_{22}) and (b) increase internal energy (via Π_{ii}). Thus in this phase ($\frac{St}{\sqrt{Mg_0}} < 2$), both Π_{22} and Π_{ii} must be negative, and this is evident in Figs. 23 and 25. Once the initial disparity between $\overline{u_2 u_2}/2$ and internal energy is removed, the same equi-partitioning tendency of pressure fluctuations now ($\frac{St}{\sqrt{Mg_0}} \geq 2$) causes simultaneous increase in both internal energy and $\overline{u_2 u_2}$. This can be seen in Fig. 17 as well. This simultaneous increase in stream-normal kinetic energy and internal energy is realized by negative pressure dilatation (Fig. 25) and positive Π_{22} (Fig. 23) in the WC and LM regimes.

4 Summary and conclusions

In rapidly sheared homogeneous compressible turbulence, it is known that kinetic energy exhibits three distinct evolution regimes depending on the value of gradient Mach number [28]. We label the three stages as pressure-released (PR), wave-character (WC) and sub-sonic low-Mach number (LM) regimes in decreasing order of Mach number. In this paper, we characterize the behavior of flow and thermodynamic fluctuations in these regimes and examine flow-thermodynamics interactions. The main findings of the paper are now listed.

1. **Mach number of relevance:** The appropriate Mach number for characterizing RDT behaviour can be gleaned by an examination of (16). It is clear that velocity amplitude of a given mode depends upon wavenumber and mean strain-rate. This observation leads us to define the RDT gradient Mach number as:

$$Mg(t) = \frac{S}{a\,|\kappa|} \tag{24}$$

   where $|\kappa|$ is the characteristic wavenumber at a given time t.
2. **Time-scales of relevance:** Turbulent kinetic energy growth is examined in acoustic and mixed acoustic-shear times. In previous studies [25,28] the growth was investigated in shear time leading to the conclusion that turbulence could grow faster for lower initial gradient Mach number than for larger initial gradient Mach number. In acoustic (real) time, it is clearly demonstrated that larger initial gradient Mach number lead to more rapid growth. It is the shear normalization of time that leads to the impression of more rapid growth in low Mach number flows.

3. **Evolution of flow variables:** Kinetic energy grows very rapidly in PR regime, very slowly in WC stage and exhibit nearly incompressible evolution rate in the final LM stage. Streamwise fluctuations mirror this behavior. However, stream-normal fluctuations exhibit a very different trend. They experience depletion in the PR regime and subsequently rapid oscillatory growth in WC and LM stages. The transverse fluctuations grow only during the LM stage in a manner similar to incompressible shear turbulence. It must be noted that stream-normal fluctuations are dilatational in nature and the other two components are largely solenoidal. In DNS calculations (e.g., [26]) this uninhibited growth of thermodynamic fluctuations is not observed. Indeed, even in a viscous RDT simulation (unpublished work), the thermodynamic fluctuations decline at late times. The explanation is straight-forward—viscous effect acts preferentially on the dilatational fluctuations due to their smaller length-scale. Recall that the length-scale associated with dilatational field is given by $1/\kappa_2$. As κ_2 grows with time, the dilatational length-scale gets smaller and viscosity dissipates these fluctuations very rapidly. The solenoidal field—which is orthogonal to κ_2—is associated with longer length scale and consequently is not dissipated as rapidly. As dilatation vanishes, the mechanism of energy transfer from mechanical to thermodynamic fluctuations—pressure-dilatation—also diminishes leading to a reduction and ultimate disappearance of thermodynamic fluctuations.
4. **Evolution of thermodynamic state variables:** Density and temperature fluctuations grow slowly in PR regime and then very rapidly in WC and LM regimes. Interestingly, they continue to grow even at low M_g values. This is due to the fact that any initial dilatation present in the incompressible regime cannot be eliminated by the effects of pressure in RDT physics. At low Mach numbers, pressure will preserve incompressibility only in the absence of any initial dilatational field. If a dilatational field is initially present, even at low Mach numbers, density fluctuations can survive in the flow field. As discussed in the last passage, in DNS studies, pressure-dilatation will diminish at later times due to viscous effects.
5. **Flow-thermodynamics interactions:** The interactions manifest *via* pressure-strain correlation tensor (Π_{ij}) and pressure-dilatation (Π_{kk}). In all three regimes, pressure-dilatation acts to bring about equipartition between dilatational kinetic energy and internal energy. The individual pressure-strain tensor components behave differently in the three stages. In the PR stage, Π_{11} and Π_{22} are negative indicating energy transfer from $\overline{u_1u_1}$ and $\overline{u_2u_2}$ to internal energy. In WC and LM regimes Π_{22} becomes positive and Π_{33} is also positive and non-negligible. Thus the energy transfer in the final two stages are from $\overline{u_1u_1}$ to $\overline{u_2u_2}$, $\overline{u_3u_3}$ and internal energy.

In summary, this study carefully characterizes the behavior of flow and thermodynamic fluctuations in high Mach number shear turbulence. While these observations and inferences are of intrinsic interest, further analysis is needed to clearly explicate the underlying physical mechanisms. In a follow-up study [3], we examine the influence of initial temperature fluctuations, turbulent Mach number and dilatational field on the turbulence evolution. With the introduction of initial thermodynamic fluctuations the basic three-stage behavior remains intact. It is found that these fluctuations only influence the onset and the duration of various regimes. By suitably manipulating the thermal fluctuations one can prolong or curtail the stabilizing second regime. Variations in turbulent Mach number do not significantly alter the onset or duration of the various regimes.

Acknowledgments This work was supported by AFOSR (MURI) Grant no. FA9550-04-1-0425 (Program Manager: Dr. John Schmisseur) and by the National Defense Science and Engineering Graduate (NDSEG) Fellowship through the High Performance Computing agency with the Department of Defense, and AFOSR-NASA National Science Research Center for Hypersonic Laminar-Turbulent Transition.

References

1. Adumitroaie, V., Ristorcelli, J.R., Taulbee, D.B.: Progress in favre-reynolds stress closures for compressible flows. Phys. Fluids **11**, 2696–2719 (1999)
2. Batchelor, G.K., Proudman, I.: The effect of rapid distortion of a fluid in turbulent motion. Q. J. Mech. Appl. Math. **7**, 121–152 (1954)
3. Bertsch, R.L.: Rapidly-sheared compressible turbulence: characterization of different pressure regimes and effect of thermodynamic fluctuations. Master's thesis, Texas A&M University (2010)
4. Blaisdell, G.A., Coleman, G.N., Mansour, N.N.: Rapid distortion theory for compressible homogenous turbulence under isotropic mean strain. Phys. Fluids **8**, 2692 (1996)
5. Bradshaw, P.: Compressible turbulent shear flows. Ann. Rev. Fluid Mech. **9**, 33–54 (1977)
6. Brethouwer, G.: The effect of rotation on rapidly sheared homogeneous turbulence and passive scalar transport. Linear theory and direct numerical simulations. J. Fluid Mech. **542**, 305–342 (2005)
7. Cambon, C., Coleman, G.N., Mansour, N.N.: Rapid distortion analysis and direct simulation of compressible homogeneous turbulence at finite mach number. J. Fluid Mech. **257**, 641–665 (1993)

8. Durbin, P.A., Zeman, O.: Rapid distortion theory for homogenous compressed turbulence with application to modeling. J. Fluid Mech. **242**, 349 (1992)
9. Girimaji, S.S., Jeong, E., Poroseva, S.V.: Pressure-strain correlation in homogeneous anisotropic turbulence subject to rapid straindominated distortion. Phys. Fluids **15**, 3209–3222 (2003)
10. Girimaji, S.S., O'Neil, J.R., Yu, D.: Rapid distortion analysis of homogeneous turbulence subjected to rotating shear. Phys. Fluids **18**, 085102-1–085102-13 (2006)
11. Heinz, S.: A model for the reduction of the turbulent energy redistribution by compressibility. Phys. Fluids **15**, 3580–3583 (2003)
12. Hunt, J.C.R., Carruthers, D.J.: Rapid distortion theory and the 'problems' of turbulence. J. Fluid Mech. **212**, 497–532 (1990)
13. Jackson, T.L., Grosch, C.E.: Absolute/convective instabilities and the convective mach number ina compressible mixing layer. Phys. Fluids A **2**, 949–954 (1990)
14. Kassinos, S.C., Reynolds, W.C.: A particle representation model for the deformation of homogeneous turbulence. Annual Research Briefs (Center for Turbulence Research, NASA Ames/Stanford University), Stanford, CA, pp. 31 (1996)
15. Kline, S.J., Cantwell, B.J., Lilley G.M.: The 1980–81 AFOSR-HTTM-stanford conference on complex turbulent flows. Stanford University, CA (1981)
16. Lavin, T.: Rapid distortion theory for compressible turbulence. Master's thesis, Texas A&M University (2007)
17. Lee, K., Girimaji, S.S.: Flow-thermodynamics interactions in rapidly sheared compressible turbulence. Under Rev. Theor. Comput. Fluid Dyn.
18. Livescu, D., Jaberi, F.A., Madnia, C.K.: The effects of heat release of the energy exchange in reaching turbulent shear flow. J. Fluid Mech. **450**, 35–66 (2002)
19. Livescu, D., Madnia, C.K.: Small scale structure of homogenous turbulent shear flow. Phys. Fluids **16**, 2864 (2004)
20. Mee, D.J.: Boundary layer transition measurement in hypervelocity flows in a shock tunnel. 39th AAAA Aerospace Sciences Meeting and Exhibit, Reno, Nevada, USA, pp. 8–1 (2001)
21. Mishra, A.A., Girimaji, S.S.: Pressure-strain correlation modeling: towards achieving consistency with rapid distortion theory. Flow Turbul. Combust. **85**, 593–619 (2010)
22. Papamoschou, D., Roshko, A.: The compressible turbulent shear layer: an experimental study. J. Fluid Mech. **197**, 453–477 (1999)
23. Pope, B.: Turbulent flows. Cambridge University Press, Cambridge, UK (2000)
24. Roy, C.J., Blottner, F.G.: Review and assessment of tubulence models for hypersonic flows. Prog. Aerosp. Sci. **42**, 469–530 (2006)
25. Sarkar, S.: The stabilizing effect of compressibility in turbulent shear flow. J. Fluid Mech. **282**, 163–186 (1995)
26. Sarkar, S., Erlebacher, G., Hussaini, M.Y.: Direct simulation of compressible turbulence in a shear flow. Theor. Comput. Fluid Dyn. **2**, 291–305 (1991)
27. Savill, A.M.: Recent developments in rapid distortion theory. Ann. Rev. Fluid Mech. **19**, 531–573 (1987)
28. Simone, A., Coleman, G.N., Cambon, C.: The effect of compressibility on turbulent shear flow: a rapid-distortion-theory and direct-numerical-simulation study. J. Fluid Mech. **330**, 307–338 (1997)
29. Sivasubramaniyan, J., Fasel, H.F.: Numerical investigation of laminar-turbulent transition in a cone boundary layer at mach 6. 41st AIAA Fluid Dynamics Conference and Exhibit, Honolulu, Hawaii (2011)
30. Yu, H., Girimaji, S.S.: Extension of compressible ideal-gas RDT to general mean velocity gradients. Phys. Fluids **19**, 041702-1–041702-4 (2007)